

effect approach discussed here, no chemical or structural disorder is introduced, allowing us to identify the key role of the electronic doping level in determining the physical properties of these materials.

In the underdoped superconducting regime, the SO(5) theory of Zhang, as well as the theory of superconductivity in bad metals of Emery and Kivelson, predict that classical and quantum phase fluctuations are responsible for depressing T_c well below the pairing temperature, which, in these theories, is represented by T^* in Fig. 1 (5, 18). As the chemical potential μ is increased, these phase fluctuations decrease because of improved phase stiffness and screening, leading to an increase in T_c . In particular, Emery and Kivelson calculate the T_c dependence for the minimum metallicity required to suppress the phase fluctuations that prevent superconductivity from occurring. This limiting value is nonuniversal and depends on the material, the dimensionality of the system, and the details of the short-range screening. Work on YBCO single crystals, in which radiation damage was used to induce an insulating state, yields a value of $\sim 2.5 \times 10^{-3}$ ohm-cm (19, 20). In this work, we changed the metallicity directly by changing the number of carriers, finding a normal state resistivity of 2.3×10^{-3} ohm-cm. Because YBCO is highly anisotropic and quasi-2D in the underdoped regime, an equivalent 2D sheet resistance, given by the resistivity per copper oxide plane (6Å), is sometimes considered. The equivalent sheet resistance in this case is ~ 40 kohm per square, which is significantly larger than the quantum of resistance for Cooper pairs (6.45 kohm per square).

Finally, regarding the insulating state we observed, the results suggest that because the insulating state is not consistent with variable range hopping, which is what is observed at low doping levels in the antiferromagnetic Néel insulating state up to high temperatures (~ 50 K), the samples may instead be in a quantum disordered state that exists between the Néel and the superconducting ground states (21). The observed $\ln(1/T)$ behavior over the temperature range investigated suggests that this quantum disordered state may also be the state that Ando and co-workers achieved by applying large magnetic fields to underdoped LSCO (2).

References and Notes

1. A. M. Goldman and N. Markovic, *Phys. Today* **51** (no. 11), 39 (1998), and references therein; M. P. A. Fisher, G. Grinstein, S. M. Girvin, *Phys. Rev. Lett.* **64**, 587 (1990); M. P. A. Fisher, *ibid.* **65**, 923 (1990); A. F. Hebard and M. A. Paalonen, *ibid.*, p. 927; Y. Liu *et al.*, *ibid.* **67**, 2068 (1991); A. Yazdani and A. Kapitulnik, *ibid.* **74**, 3037 (1995); E. Chow, P. Delsing, D. B. Haviland, *ibid.* **81**, 204 (1998); S. L. Sondhi, S. M. Girvin, J. P. Carini, D. Shahar, *Rev. Mod. Phys.* **69**, 315 (1997); A. J. Rimberg *et al.*, *Phys. Rev. Lett.* **78**, 2632 (1997); M. I. Erements, K. Shimizu, T. C. Kobayashi, K. Amaya, *Science* **281**, 1333 (1998); G. T. Seidler, T. F. Rosenbaum, B. W. Veal, *Phys. Rev. B* **45**, 10162

- (1992); K. Karpinska *et al.*, *Phys. Rev. Lett.* **77**, 3033 (1996); N. E. Hussey *et al.*, *ibid.* **80**, 2909 (1998).
2. Y. Ando, G. S. Boebinger, A. Passner, T. Kimura, K. Kishio, *Phys. Rev. Lett.* **72**, 4662 (1995); G. S. Boebinger *et al.*, *ibid.* **77**, 5417 (1996).
3. Y. Fukuzumi, K. Mizuhashi, K. Takenaka, S. Uchida, *ibid.* **76**, 684 (1996).
4. P. Fournier *et al.*, *ibid.* **81**, 4720 (1998).
5. S.-C. Zhang, *Science* **275**, 1089 (1997).
6. C. H. Ahn *et al.*, *ibid.* **269**, 373 (1995); Y. Watanabe, *Appl. Phys. Lett.* **66**, 1770 (1995); S. Hontsu, J. Ishii, H. Tabata, T. Kawai, *ibid.* **67**, 554 (1995); S. Hontsu, M. Nakamori, H. Tabata, J. Ishii, T. Kawai, *IEEE Trans. Electron. E80-C*, 1304 (1997); C. H. Ahn *et al.*, *Appl. Phys. Lett.* **70**, 206 (1997); C. H. Ahn *et al.*, *Science* **276**, 1100 (1997); U. Kabasawa, H. Hasegawa, T. Fukazawa, Y. Tarutani, K. Takagi, *J. Appl. Phys.* **81**, 2302 (1997); L. X. Cao *et al.*, *Physica C* **47-52**, 303 (1998).
7. R. E. Glover III and M. D. Sherrill, *Phys. Rev. Lett.* **5**, 248 (1960).
8. J. Mannhart, D. G. Schlom, J. G. Bednorz, K. A. Müller, *ibid.* **67**, 2099 (1991); X. X. Xi *et al.*, *ibid.* **68**, 1240 (1992); A. Walkenhorst *et al.*, *ibid.* **69**, 2709 (1992); J. Mannhart, *Supercond. Sci. Technol.* **9**, 49 (1996).
9. A. W. Kleinsasser *et al.*, *Appl. Phys. Lett.* **55**, 1909 (1989); T. Akazaki *et al.*, *ibid.* **68**, 418 (1996); B. Mayer, J. Mannhart, H. Hilgenkamp, *ibid.*, p. 3031.
10. J.-M. Triscone *et al.*, *J. Appl. Phys.* **78**, 4298 (1996).
11. T. Terashima *et al.*, *Phys. Rev. Lett.* **67**, 1362 (1991); J.-M. Triscone and Ø. Fischer, *Rep. Prog. Phys.* **60**, 1673 (1997).
12. Off-axis scans reveal GBCO [100] (and PBCO [100])||STO [100], as well as epitaxial growth of tetragonal PZT (001) on GBCO (001), with PZT [100]||GBCO [100]. Rocking curves taken around the 005 reflection of PBCO and GBCO have typical full widths at half maximum (FWHM) of $\sim 0.09^\circ$, and rocking curves taken around the 001 reflection of PZT have a typical FWHM of $\sim 0.6^\circ$.
13. Because the primary region of interest is at low temperatures, where PBCO is insulating, the resistivity is calculated using the thickness of the GBCO layer.
14. During fabrication of the heterostructures, the ferro-

- electric layer is uniformly poled. As a result, it was not possible to measure the resistivity for the unpolarized (randomly polarized) state of the ferroelectric.
15. We believe the differences between the samples shown in Figs. 3 and 4 are due to run-to-run variations in the deposition parameters; for example, the substrate temperature and oxygenation of the samples.
16. To suppress the possible influence of the dip, the fits were carried out on the measurements taken at 7 T. Fits to the zero field data, as well as on another sample showing a superconductor-insulator transition in which the dip is not present at zero field, also yield the same conclusions.
17. Because of geometric constraints, it was not possible to measure simultaneously the size of the field effect and the carrier concentration. The Hall effect measurements described in the text were obtained on separate samples showing similar resistivities, critical temperatures, and temperature dependencies.
18. V. J. Emery and S. A. Kivelson, *Phys. Rev. Lett.* **74**, 3253 (1995); *Nature* **374**, 434 (1995). Other theories that consider phase fluctuations include S. Doniach and M. Inui, *Phys. Rev. B* **41**, 6668 (1990); D. Ariosa and H. Beck, *ibid.* **43**, 344 (1991); and T. Schneider and H. Keller, *Phys. Rev. Lett.* **69**, 3374 (1992).
19. A. G. Sun, L. M. Paulius, D. A. Gajewski, M. B. Maple, R. C. Dynes, *Phys. Rev. B* **50**, 3266 (1994).
20. Seidler *et al.*, using a magnetic field as the control parameter, have observed a critical value of 1.6×10^{-3} ohm-cm in underdoped YBCO single crystals [see (1)].
21. M. Kastner, R. J. Birgeneau, G. Shirane, Y. Endoh, *Rev. Mod. Phys.* **70**, 897 (1998); N. W. Preyer *et al.*, *Phys. Rev. B* **39**, 11563 (1989).
22. A. Carrington, A. P. Mackenzie, C. T. Lin, J. R. Cooper, *Phys. Rev. Lett.* **69**, 2855 (1992); T. Ito, K. Takenaka, S. Uchida, *ibid.* **70**, 3995 (1993).
23. We thank M. Beasley, Ø. Fischer, B. Giovannini, Y. Kagan, P. Martinoli, J. Perret, and T. Schneider for useful discussions and D. Chablaix for technical help. Supported by the Fonds National Suisse de la Recherche Scientifique.

19 January 1999; accepted 8 April 1999

Control of Hippocampal Morphogenesis and Neuronal Differentiation by the LIM Homeobox Gene *Lhx5*

Yangu Zhao,¹ Hui Z. Sheng,¹ Reshad Amini,¹ Alexander Grinberg,¹ Eric Lee,¹ SingPing Huang,¹ Masanori Taira,^{2*} Heiner Westphal^{1†}

The mammalian hippocampus contains the neural circuitry that is crucial for cognitive functions such as learning and memory. The development of such circuitry is dependent on the generation and correct placement of the appropriate number and types of neurons. Mice lacking function of the LIM homeobox gene *Lhx5* showed a defect in hippocampus development. Hippocampal neural precursor cells were specified and proliferated, but many of them failed to either exit the cell cycle or to differentiate and migrate properly. *Lhx5* is therefore essential for the regulation of precursor cell proliferation and the control of neuronal differentiation and migration during hippocampal development.

The development of Ammon's horn and the dentate gyrus of the mammalian hippocampal formation is a multistep process controlled by a complex genetic program. During embryonic development, hippocampal precursor

cells originate from the medial wall of the telencephalic vesicles. These cells proliferate in a primary germinal layer called the ventricular zone. Thereafter, they migrate out in a highly organized manner to their appropri-

REPORTS

ate target positions (1). This leads to morphogenesis of the characteristic interlocking C-shaped structures of Ammon's horn and the dentate gyrus. After migration, the postmitotic cells continue to differentiate and eventually give rise to the various types of hippocampal neurons, such as pyramidal cells, granular cells, and interneurons. Later during development, after most of the postmitotic cells have been generated, the number of proliferating cells decreases in the ventricular zone, which eventually forms an ependymal layer lining the ventricle.

Lhx5 is a member of the LIM homeobox gene family that encodes a transcription factor (2, 3). We detected *Lhx5* mRNA in the hippocampal precursor cells at embryonic day 10.5 (E10.5) and E11.5 (Fig. 1, A and B). Between E13.5 and E18.5 (E15.5 is shown in Fig. 1C), the *Lhx5* mRNA expression became restricted to the marginal zone of the developing Ammon's horn and dentate gyrus. This *Lhx5* domain corresponds to a region that contains the earliest differentiated Cajal-Retzius cells (4). Cajal-Retzius cells guide neuronal migration (5) and innervation of afferent axons (6) during the development of the hippocampal formation.

¹Laboratory of Mammalian Genes and Development, ²Laboratory of Molecular Genetics, National Institute of Child Health and Human Development, Bethesda, MD 20892, USA.

*Present address: Department of Biological Sciences, University of Tokyo, Tokyo 113, Japan.

†To whom correspondence should be addressed. E-mail: hw@helix.nih.gov

In an effort to analyze the function of *Lhx5*, we deleted part of the *Lhx5* gene encoding the second LIM domain and the homeodomain (7) in embryonic stem (ES) cells (Fig. 1, D and E). Mice heterozygous for the *Lhx5* mutation appeared normal and fertile. Homozygous offspring from crosses between the heterozygous parents were born alive and appeared normal at first. However, most of

them died within a few days after birth. At the time of weaning, only 45 out of a total of 838 progeny derived from heterozygous crosses were found to be homozygous mutants. Histological analysis of the mutant embryos revealed that the hippocampus was misformed, the choroid plexus of both the lateral ventricle and the third ventricle was missing, and the anterior callosal axons failed to cross the

Fig. 2. Defects in morphogenesis and precursor cell proliferation in the developing hippocampus of E18.5 *Lhx5* mutant embryos (B, D, and F) as compared to wild-type controls (A, C, and E). (A and B) Hematoxylin and eosin staining of coronal sections through the hippocampal region. (C and D) Proliferating cells in the hippocampal ventricular zone labeled by anti-BrdU staining. (E and F) Distribution of postmitotic cells born at E13.5 in the hippocampal region of E18.5 embryos. Arrows in (A) through (F) point at the hippocampal ventricular zone. Scale bar in (E) represents 100 μ m for (C) and (D) and 250 μ m for (A), (B), (E), and (F). ah, Ammon's horn; dg, dentate gyrus; th, thalamus. To label proliferating cells, pregnant females were injected intraperitoneally with BrdU (100 μ g per gram of body weight, dissolved in 0.9% NaCl) and killed 2 hours later. Embryos were dissected and fixed (27). Frozen sections (10 μ m) were treated with 2M HCl and neutralized in sodium borate. BrdU was detected with an alkaline phosphatase-labeled antibody to BrdU (1 U/ml, Boehringer Mannheim). A similar procedure was followed for birth dating analysis, except that BrdU was injected at E13.5 and the embryos were collected at E18.5.

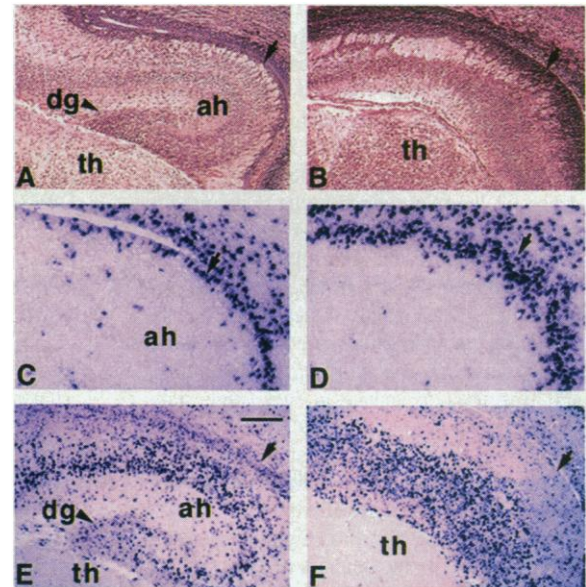
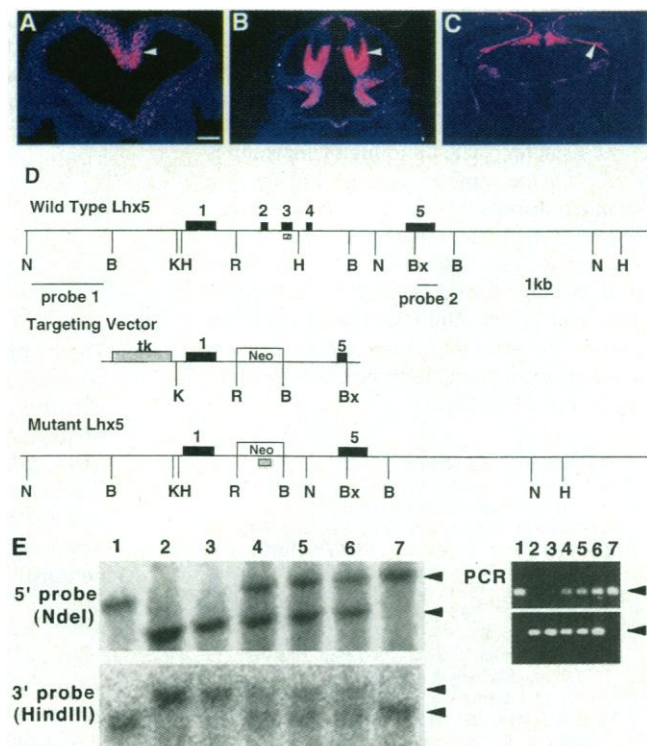


Fig. 1. *Lhx5* expression in the developing hippocampus and its targeted deletion. Expression of *Lhx5* mRNA in the developing hippocampus at E10.5 (A), E11.5 (B), and E15.5 (C) detected by in situ hybridization (27). (D) Through homologous recombination in ES cells, exons 2, 3, and 4 of the *Lhx5* gene (top, numbered black boxes) encoding the second LIM domain and the homeodomain (7) were replaced by the *Neomycin* (*Neo*) gene (bottom) derived from the targeting vector (middle). (E) Southern (DNA) blotting and polymerase chain reaction (PCR) analyses of DNA of E18.5 embryos derived from a heterozygous mating. After *Nde* I digestion, a 5' probe detected a 13.5-kb band for the wild-type *Lhx5* allele and a 11.0-kb band for the targeted allele (arrowheads). Hybridization of *Hind* III-digested DNA with a 3' probe revealed a 12.5-kb band for the wild-type allele and a 14.6-kb band for the mutant allele (arrowheads). With the same DNA samples as templates, PCR (using a pair of primers from the third exon of *Lhx5* and a pair of primers from *Neomycin*) amplified a 250-base pair (bp) fragment from the wild-type allele (top) and a 500-bp fragment from the mutant allele (bottom), respectively. Lanes 1 and 7, 4 through 6, and 2 and 3 represent samples from wild-type, heterozygous, and homozygous embryos, respectively. Scale bar in (A) represents 100 μ m for (A) and 240 μ m for (B) and (C). B, Bam HI; Bx, Bstx I; H, Hind III; K, Kpn I; N, Nde I; R, Eco RI. The targeting vector was constructed by replacing exons 2, 3, and 4 of the *Lhx5* gene with a neomycin-resistance gene flanked by 2.3 kb (5') and 2.5 kb (3') of homologous sequences and by the thymidine kinase gene. The vector was linearized and electroporated into the R1 line of ES cells (28). Clones resistant to G418 (350 μ g/ml) and gancyclovir (2 mM) double selection were screened by Southern hybridization with both a 5' probe and a 3' probe outside the flanking homologous sequences. The ES cells heterozygous for the targeted *Lhx5* allele were injected into 129/Sv blastocysts to generate chimeric mice that transmitted the *Lhx5* deletion through the germline. Chimeric mice were mated to wild-type CD1 to generate heterozygous animals that were crossed to produce F₂ offspring for analysis.



REPORTS

midline. Although these defects may not cause the lethality, the cyanotic appearance of dying animals suggested to us additional defects in respiratory control centers. However, we were unable to detect morphological defects either in the hindbrain or in other discrete regions of the forebrain (including the neocortex, basal ganglia, thalamus, and hypothalamus), midbrain, and spinal cord where *Lhx5* is normally expressed. The cytoarchitectonic organization of all these regions appeared normal in mutant embryos as compared to wild-type controls. It is possible that functional compensation for *Lhx5* is ren-

dered, at least in part, by *Lhx1*, a closely related LIM homeobox gene that is coexpressed with *Lhx5* in these regions (2).

At E18.5, the *Lhx5* homozygous mutant embryos showed histological defects in the hippocampal regions (Fig. 2, A and B). The ventricular zone was thicker than normal. Numerous cells were clustered in a region ventral to the lateral ventricle, but these cells failed to form the morphologically distinctive structures of Ammon's horn and the dentate gyrus. The fimbria and the hippocampal commissure, two major axon tracts of the hippocampal formation, were entirely missing from the mutant

embryos. Consistent with the thickening of the hippocampal ventricular zone, bromodeoxyuridine (BrdU) pulse labeling at E18.5 showed that the number of proliferating cells in the mutant hippocampal ventricular zone was increased as compared to that in the wild-type control (Fig. 2, C and D). Using BrdU labeling, we also marked cells undergoing their final cell division at E13.5. By E18.5, many BrdU-labeled postmitotic cells were observed in the hippocampal region of mutant embryos (Fig. 2F). These cells migrated out of the ventricular zone, but they failed to position themselves properly to form the distinctive structures of Ammon's horn and the dentate gyrus that were observed in wild-type embryos (Fig. 2E).

By E18.5, the transcript of the LIM homeobox gene *Lhx2* was detected in both the ventricular zone and the differentiation zone of Ammon's horn and the dentate gyrus in wild-type embryos (Fig. 3A). The expression of *Lhx2* in the ventricular zone is consistent with its role in the proliferation of the hippocampal precursor cells (8). The *Lhx2* expression in the differentiation zone suggests that this gene may also support neuronal differentiation in the developing hippocampus. In *Lhx5* null mutant embryos, *Lhx2* mRNA was detected in the thickened ventricular zone but not in postmitotic cells that had migrated out of the ventricular zone (Fig. 3B). At this stage, different types of hippocampal neurons could be identified in wild-type embryos by specific markers. Pyramidal cells in Ammon's horn were labeled by an antibody to glutamate receptor subunit GluR1 (Fig. 3C). Interneurons were stained for glutamate decarboxylase GAD67 (Fig. 3E). Granule cells in the dentate gyrus and the Cajal-Retzius cells were visualized with an antibody specific for the calcium-binding protein calretinin (Fig. 3G). In contrast, immunostaining for GluR1 (Fig. 3D), GAD67 (Fig. 3F), and calretinin (Fig. 3H) was diminished in comparable regions of the *Lhx5* mutant embryos. However, postmitotic cells in these fields were stained in both wild-type (Fig. 3, I and K) and mutant (Fig. 3, J and L) embryos by antibodies directed against general neuronal markers such as class III β -tubulin (9), the microtubule associate protein MAP2, and the glial cell marker glial fibrillary acidic protein (GFAP). Thus, these postmitotic cells were initially able to acquire certain identities of neurons or glial cells, but they did not differentiate further into the various subclasses of hippocampal neurons in the absence of *Lhx5* function. In order to determine whether the disruption of differentiation of these cells was accompanied by apoptosis, TUNEL (10) staining was performed. As in wild-type embryos, very few apoptotic cells were detected in mutant hippocampal regions.

Early in development, several homeobox genes, including *Lhx2*, *Emx2*, and *Otx1*, are expressed in the developing hippocampal anlagen, and some of these genes are required

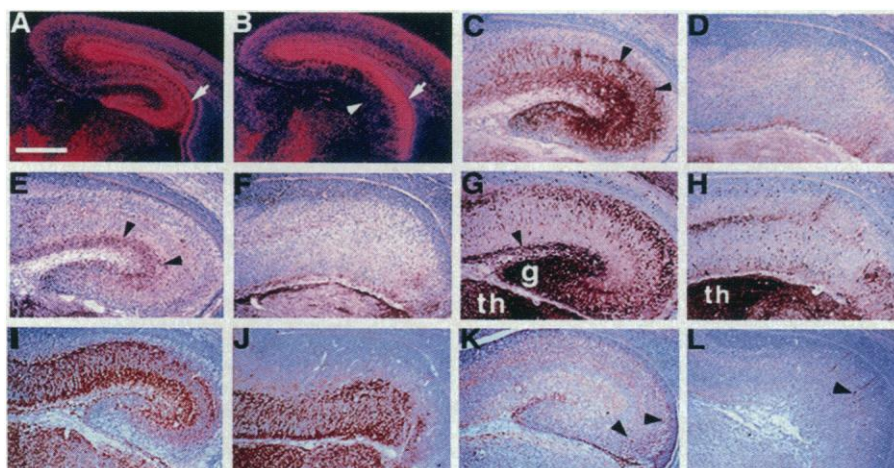


Fig. 3. Impaired hippocampal neuronal differentiation in *Lhx5* mutant embryos. Expression of various molecular markers in the hippocampal regions in E18.5 wild-type (A, C, E, G, I, and K) and *Lhx5* mutant embryos (B, D, F, H, J, and L). (A and B) Expression of *Lhx2* mRNA detected by in situ hybridization (27). (C through L) Immunohistochemical staining of GluR1 (C and D), GAD67 (E and F), calretinin (G and H), MAP2 (I and J), and GFAP (K and L). Arrows in (A) and (B) point at the hippocampal ventricular zone. Arrowhead in (B) points at the postmitotic cells that migrated out of the ventricular zone. Arrowheads in (C), (E), and (G) point at labeled pyramidal cells, interneurons, and the Cajal-Retzius cells, respectively. Arrowheads in (K) and (L) point at cells positive for GFAP. Scale bar in (A) represents 380 μ m for (A) and (B) and 200 μ m for (C) through (L). g, granule cells of the dentate gyrus; th, thalamus. For immunohistochemistry, frozen sections (10 μ m) from paraformaldehyde-fixed samples were incubated with primary antibodies. Reacting antigens were detected with the ABC elite kit (Vector Lab) or the histomouse kit (Zymed). The primary antibodies were as follows: anti-GluR1 (1 μ g/ml), anti-GAD67 (1:1000, Chemicon), anti-calretinin (1:1500, RDI), anti-MAP2 (1:250, Sigma), and anti-GFAP (1:500, DAKO).

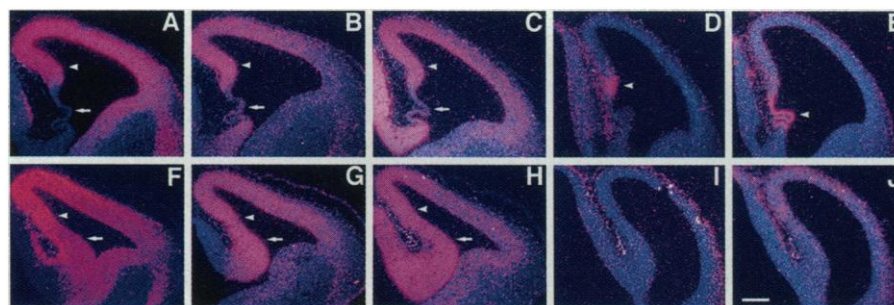


Fig. 4. Specification of hippocampal precursor cells in *Lhx5* mutant embryos. Expression of *Lhx2* (A) and (F), *Emx2* (B) and (G), *Otx1* (C) and (H), *Wnt5a* (D) and (I), and *Bmp7* (E) and (J) in E12.5 wild-type (A through E) and *Lhx5* homozygous (F through J) embryos detected by in situ hybridization (27). Arrowheads in (A) through (C) and (F) through (H) point at the hippocampal anlagen. Arrows in (A) through (C) and (F) through (H) point at the choroid plexus in a wild-type embryo and the ventrally expanded hippocampal domain in a mutant embryo, respectively. Arrowheads in (D) and (E) point at the regions where *Wnt5a* (D) and *Bmp7* (E) were expressed. Scale bar in (J) represents 200 μ m for all panels.

for the specification of the region (8, 11, 12). We examined the expression of these genes in *Lhx5* mutant embryos. At E12.5, all three of these genes were expressed in the hippocampal anlagen in both wild-type (Fig. 4, A through C) and mutant (Fig. 4, F through H) embryos, which indicates that the hippocampal precursor cells were specified after disruption of *Lhx5*. In the mutant embryos, the domains of *Lhx2*, *Emx2*, and *Otx1* expression expanded ventrally into the region of the telencephalic choroid plexus, and morphogenesis of the choroid plexus was impaired. Signaling molecules of the *Wnt* and *Bmp* families have been implicated in patterning the medial telencephalic wall to form the hippocampal anlagen and the choroid plexus, because these molecules are expressed at the border between these two morphologically distinctive structures (13, 14) (Fig. 4, D and E). In support of this idea, expression of *Wnt5a* (Fig. 4I), *Bmp4*, and *Bmp7* (Fig. 4J) was diminished in this specific region in *Lhx5* null mutant embryos.

Previous experiments have shown that other members of the LIM homeobox gene family play crucial roles in the differentiation of distinct cell types in various organisms (15–18). In mice, for example, *Islet1* is essential for the differentiation of motor neurons in the spinal cord (15), and *Lhx3* is required for the differentiation of the pituitary cell lineages (16). More recently, it has been observed that *Lhx3* and *Lhx4* together control the axon projection of subtypes of motor neurons as well as their exact soma position in the developing spinal cord (17). Our data suggest that *Lhx5* may play an analogous role in the developing forebrain.

Defects in hippocampal development have been observed in mice carrying null mutations in a variety of genes. Functional ablation of the homeobox gene *Emx2* (11) or *Lhx2* (8) leads to an early arrest of hippocampal development as precursor cells fail to be specified or to proliferate. Mutations in *Reeler* (5), *Mdab1* (19), *Cdk5* (20), *P35* (21), and *Pafah1b1* (22) impair neuronal migration, resulting in a disorganization of cells in Ammon's horn and the dentate gyrus. Our results show that *Lhx5* is required for differentiation of the various types of hippocampal neurons. Together, these studies reveal an intricate genetic program underlying the assembly of complex hippocampal structures.

Expression of *Lhx5* after E13.5 in the Cajal-Retzius cells raises the possibility that the impairment in hippocampal morphogenesis observed in *Lhx5* mutant embryos could result from a lack of function of those cells. The gene *Reeler* is expressed in these cells (5), in keeping with the possibility that this gene might be a downstream target of *Lhx5*. However, the defects in morphogenesis as well as in neuronal differentiation of Ammon's horn and the dentate gyrus seen in the *Lhx5* mutant embryos are

more severe than those of *Reeler* (5), *Mdab1* (19), *Cdk5* (20), *P35* (21), and *Pafah1b1* (22) mutants, which suggests that *Lhx5* may control a different pathway. The *Lhx5* knockout mice provide a model to further understand the molecular and cellular mechanisms underlying the formation of Ammon's horn and the dentate gyrus and their functions in cognition, learning, and memory.

References and Notes

1. V. S. Caviness Jr., *J. Comp. Neurol.* **151**, 113 (1973); B. B. Stanfield and W. M. Cowan, *ibid.* **185**, 423 (1979); S. A. Bayer, *ibid.* **190**, 115 (1980).
2. H. Z. Sheng et al., *Dev. Dyn.* **208**, 266 (1997).
3. R. Toyama et al., *Dev. Biol.* **170**, 583 (1995).
4. E. Soriano, J. A. Del Rio, A. Martinez, H. Super, *J. Comp. Neurol.* **342**, 571 (1994).
5. G. D'Arcangelo et al., *Nature* **374**, 719 (1995); K. Nakajima, K. Mikoshiba, T. Miyata, C. Kudo, M. Ogawa, *Proc. Natl. Acad. Sci. U.S.A.* **94**, 8196 (1997).
6. J. A. Del Rio et al., *Nature* **385**, 70 (1997).
7. S. Bertuzzi et al., *Genomics* **36**, 234 (1996).
8. F. D. Porter et al., *Development* **124**, 2935 (1997).
9. Neuron-specific class III β -tubulin was detected by Tuj-1 antibody (BabCO, 1:5000).
10. TUNEL staining was performed on paraffin sections with a Neuro TACS II kit (Trevigen).
11. M. Pellegrini, A. Mansouri, A. Simeone, E. Boncinelli, P. Gruss, *Development* **122**, 3893 (1996); M. Yoshida et al., *ibid.* **124**, 101 (1997).
12. A. Simeone et al., *EMBO J.* **12**, 2735 (1993).
13. E. A. Grove, S. Tole, J. Limon, L. Yip, C. W. Ragsdale, *Development* **125**, 2315 (1998).
14. Y. Furuta, D. W. Piston, B. L. M. Hogan, *ibid.* **124**, 2203 (1997).
15. S. L. Pfaff, M. Mendelsohn, C. L. Stewart, T. Edlund, T. M. Jessell, *Cell* **84**, 309 (1996).

16. H. Z. Sheng et al., *Science* **272**, 1004 (1996).
17. K. Sharma et al., *Cell* **95**, 817 (1998).
18. I. B. Dawid, J. J. Breen, R. Toyama, *Trends Genet.* **14**, 156 (1998); J. C. Way and M. Chalfie, *Cell* **54**, 5 (1988); G. Freyd, S. K. Kim, H. R. Horvitz, *Nature* **344**, 876 (1990); O. Hobert et al., *Neuron* **19**, 345 (1997); O. Hobert, T. D'Alberti, Y. Liu, G. Ruvkun, *J. Neurosci.* **18**, 2084 (1998); C. Bourgouin, S. E. Lundgren, J. B. Thomas, *Neuron* **9**, 549 (1992).
19. M. Sheldon et al., *Nature* **389**, 730 (1997); B. W. Howell, R. Hawkes, P. Soriano, J. A. Cooper, *ibid.*, p. 733.
20. T. Ohshima et al., *Proc. Natl. Acad. Sci. U.S.A.* **93**, 11173 (1996).
21. T. Chae et al., *Neuron* **18**, 29 (1997).
22. S. Hirotsune et al., *Neuron Genet.* **19**, 333 (1998).
23. G. W. Robinson, S. Wray, K. A. Mahon, *New Biol.* **3**, 1183 (1991).
24. A. Simeone et al., *EMBO J.* **11**, 2541 (1992).
25. Y. Xu et al., *Proc. Natl. Acad. Sci. U.S.A.* **90**, 227 (1993).
26. B. J. Gavin, J. A. McMahon, A. P. McMahon, *Genes Dev.* **4**, 2319 (1990).
27. Embryos were fixed with 4% paraformaldehyde by immersion (E10.5 to E12.5) or transcardial perfusion (E15.5 to E18.5) and embedded in paraffin. Sections (5 μ m) were cut and processed for in situ hybridization by published procedures (23). The probes used for in situ hybridization were specific for *Emx2* (24), *Lhx2* (25), *Lhx5* (2), *Otx1* (12), *Wnt5a* (26), *Bmp4*, and *Bmp7* (14).
28. A. Nagy, J. Rossant, R. Nagy, W. Abramow-Newerly, J. C. Roder, *Proc. Natl. Acad. Sci. U.S.A.* **90**, 8424 (1993).
29. We thank E. Boncinelli for *Otx1* and *Emx2* probes, B. L. Hogan for *Bmp4* and *Bmp7* probes, F. D. Porter for the *Lhx2* probe, A. McMahon for the *Wnt5a* probe, R. Wenthold for the antiserum to GluR1, and X. Jian, K. Pfeifer, S. Shtrom, A. Tomac, and M. Fiorenza for comments on the manuscript.

3 December 1998; accepted 15 April 1999

Separate Signals for Target Selection and Movement Specification in the Superior Colliculus

Gregory D. Horwitz and William T. Newsome*

At any given instant, multiple potential targets for saccades are present in the visual world, implying that a "selection process" within the brain determines the target of the next eye movement. Some superior colliculus (SC) neurons begin discharging seconds before saccade initiation, suggesting involvement in target selection or, alternatively, in postselectional saccade preparation. SC neurons were recorded in monkeys who selected saccade targets on the basis of motion direction in a visual display. Some neurons carried a direction-selective visual signal, consistent with a role in target selection in this task, whereas other SC neurons appeared to be more involved in postselection specification of saccade parameters.

The primate SC plays a major role in the generation of saccades. Many neurons in the intermediate and deep layers of the SC fire a

brief burst of action potentials starting approximately 20 ms preceding saccades of a particular range of directions and amplitudes; the region defined by the end points of such saccades comprises the "movement field" of an SC neuron. For each neuron, the location of the movement field in space varies systematically with the location of the neuron in the SC (1–4). Many SC neurons exhibit a "pre-

Howard Hughes Medical Institute and Department of Neurobiology, Stanford University School of Medicine, Stanford, CA 94305, USA.

*To whom correspondence should be addressed. E-mail: bill@monkeybiz.stanford.edu